Investigating the Effects of DEM Error in Scaling Analysis

Timothy D. James, Patrice E. Carbonneau, and Stuart N. Lane

Abstract

Digital elevation models (DEMs) are prone to error that, as they can never be entirely eliminated, must be managed effectively. Thus, it is important to understand the nature of error and their sources, especially in the context of the intended use of a DEM. This paper investigates the effects that can be expected when common DEM errors propagate through a scaling analysis. The errors investigated include those associated with perturbation of camera exterior orientation parameters, focal length, and DEM image coordinates, which were simulated numerically. The role of detrending was also investigated. Scaling analysis, by way of the fractal dimension, using a new two-dimensional approach was carried out on a variety of surfaces before and after the introduction of error and the application of detrending. The results reveal some serious procedural implications on scaling analysis and cast doubt on the authenticity of some scaling analysis results in the absence of robust quality assessment and of independent supporting evidence.

Introduction

Like any measurement, digital elevation models (DEMs) are prone to error associated with the methods and conditions of their generation. Although error can never be entirely eliminated, it can be minimized and must be managed effectively. Thus, there is always a need to understand how the presence of error will affect DEM data. However, perhaps more important is how error will affect information derived from DEM data on which conclusions are based (Wise, 1998). This proactive approach to data collection and analysis will enable users of topographic data to make informed decisions about how best to quantify, to prevent, to correct or to accept any errors in a dataset. This has been addressed in conventional data collection and applications (e.g., Gong *et al.*, 2000; Huang, 2000; Wolf and Dewitt, 2000). However, the development of automated digital methods has produced a change in the nature of DEM error and in the way topographic data is applied.

The availability of large, high-resolution datasets has made possible the description and quantification of surface characteristics across a large range of scales in a single dataset. Scaling analysis is a method used to describe how the elevation change of a surface varies as a function of scale. It is an important type of analysis, as it can provide additional information about a surface including the nature of the physical processes that have acted over time (Butler *et al.*, 2001). There are many ways this can be accomplished (see Klinkenberg, 1994; Klinkenberg and Goodchild, 1992), but all methods involve comparing the change of some parameter (i.e., elevation) against a change in scale (i.e., distance between points on a grid). In many cases, the scaling characteristics of natural surfaces obey a power law, which can be quantified by estimating the fractal dimension (*D*) (e.g., Butler *et al.*, 2001; Nikora *et al.*, 1998; Robert, 1991; Robert and Richards, 1988). Russ (1994) explains that a surface with fractal characteristics has irregularities at all scales, and when magnified reveals more detail showing the same characteristics as the whole. *D* is a parameter used to quantify this phenomenon and is discussed at length in Mandelbrot (1967), Mandelbrot (1982), and Russ (1994). In terms of topography, it is potentially important as a means of estimating river bed roughness (Helmlinger *et al.*, 1993), which is a key parameter as it influences many river processes including average flow, turbulence, flow resistance, and sediment transport (Butler *et al.*, 2001; Griffiths, 1989; Hey, 1988). It can also be important for understanding processes relevant in aquatic habitats (i.e., Nikora *et al.*, 1998) and in DEM quality assessment exercises (i.e., Carbonneau *et al.*, 2003). However, the effects of even common errors on the results of scaling analyses are not well understood. Since the quality of parameters derived from a DEM depends, not only on the magnitude of error but also on its structure (Heuvelink, 1998; Hunter and Goodchild, 1997; Lee *et al.*, 1992), it is important that the effect of error on scaling analysis be investigated further.

Aim and Objectives

This research aimed to investigate the effects that can be expected when common DEM errors propagate through a scaling analysis. The research objectives were: (a) to use numerical modeling to simulate common photogrammetric

Timothy D. James is at the School of Environment and Society, University of Wales, Swansea, SA3 5LQ, UK and formerly at the School of Geography, University of Leeds, Leeds, LS2 9PS, UK (t.d.james@swansea.ac.uk).

Patrice E. Carbonneau is at the Department of Geography, Durham University, Durham, DH1 3LE, UK and formerly at the Institut National de la Recherche Scientifique, Centre Eau, Terre et Environement, 490 rue da la Couronne, Québec, Canada (patrice.carbonneau@durham.ac.uk).

Stuart N. Lane is at the Department of Geography, Durham University, Durham, DH1 3LE, UK and formerly at the School of Geography, University of Leeds, Leeds, LS2 9PS, UK (s.n.lane@durham.ac.uk).

Photogrammetric Engineering & Remote Sensing
Vol. 73, No. 1, January 2007, pp. 067–078.

0099-1112/07/7301–0067/$3.00/0

errors and to apply these to a variety of surfaces with known scaling characteristics; (b) to apply scaling analysis to these surfaces both before and after error was applied using a new, automated routine that robustly estimates D in two dimensions across a surface; (c) to determine the nature of the effect of simulated errors on scaling analysis which includes the prerequisite routines required to remove surface trend; and (d) to consider the general implications of the findings on the application of scaling analysis to DEMs of natural surfaces. The experiment focused on the effects of some simple but common error sources encountered in photogrammetry including error in: (a) positional and rotational components of the exterior orientation parameters; (b) sensor focal length; and (c) DEM image coordinates. The errors were simulated through numerical modeling and were applied to an artificially generated surface designed to mimic the scaling characteristics of a natural surface under controlled conditions. The effect of the simulated error and of detrending on the outcome of scaling structure of the surface was ascertained by comparing the results of the analysis applied under a variety of conditions.

Scaling Analysis and the Fractal Dimension

In terrain modeling, scaling analysis is often used to quantify how the elevation of a surface varies as a function of scale. When the relationship between horizontal distance and elevation difference obeys a power law, the surface is said to be statistically self-similar across the range over which the power law holds (Mandelbrot, 1982). However, since scaling in nature is usually different in the horizontal and vertical directions (Mark and Aronson, 1984), the term *self-affinity* is used to describe more accurately the scaling characteristics of natural surfaces (Goodchild and Mark, 1987; Roy *et al.*, 1987). In addition, self-affinity can also vary with direction. If this is the case, the surface is said to be anisotropic while one that is constant with direction is said to be isotropic (Russ, 1994).

Hobson (1972) explained that for a parameter to be useful for the quantification of morphology, it must be conceptually descriptive, easily measurable, and applicable over a range of scales. An approach that meets these requirements in the presence of self-affinity is based on fractal geometry and the estimation of the fractal dimension (D) (Mandelbrot, 1967). In practice, self-affinity has been found to exist over a range of different scales which can yield overlapping fractal bands (Biham *et al.*, 1998). These are often called *mixed fractals* or *multifractals*. However, as Russ (1994) points out, these term can have different meanings including where several geomorphological processes have operated: (a) over discrete bands allowing distinct bands of scale-invariance to be differentiated (Suzuki, 1984); and (b) with overlapping bands, sometimes where one fractal surface has been superimposed on another, to produce a spectrum of D values (Weissel *et al.*, 1994). Although, some uncertainly remains over the most suitable terminology to describe these phenomena, for the purposes of this research, *mixed fractal* will be used to refer to (a), where several fractal bands can be identified.

In the context of natural surfaces, it is important that a method for estimating D is chosen that: (a) produces robust estimates of D; (b) is suitable for self-affine data; (c) detects both isotropy and anisotropy; (d) is robust when applied to non-Gaussian and non-stationary data; and (e) recognizes the existence of mixed fractals. Butler (1999) conducted a comprehensive review of the various methods of estimating D with respect to this criteria and found that the semi-variogram method emerged as the most suitable for achieving these objectives. It has been used in a variety of applications in the natural sciences (e.g., Burrough, 1981; Butler *et al.*, 2001; Helmlinger *et al.*, 1993; Klinkenberg and Goodchild, 1992; Mark and Aronson, 1984; Oliver and Webster, 1986; Robert, 1988; Robert, 1991; Roy *et al.*, 1987) particularly for describing the spatial variation within a dataset in terms of magnitude, scale, and general form (Oliver and Webster, 1986). Although research has cautioned against using this approach for estimating D for very rough surfaces (i.e., where $D \rightarrow 3$), this condition is rare in natural surfaces (Tate, 1998). Research has also demonstrated that the variation in estimates of D is largely a function of the method used (Klinkenberg and Goodchild, 1992). These uncertainties, like those found by Wen and Sinding-Larsen (1997), become irrelevant when calculating relative estimates of D. Russ (1994) emphasizes that it is often more important to determine the differences between surfaces using the same method. Therefore, the semi-variogram method of estimating D was deemed the most suitable for use in this research.

The Semi-variogram

Originally, the semi-variogram was developed for mining purposes (David, 1977; Journel and Huijbregts, 1978) to express the semi-variance (γ) between the elevation of point pairs as a function of the horizontal distance or lag (τ) between them. In practice, the semi-variance of a surface is expressed at each lag in a semi-variogram. Using a DEM on a regular grid, it is computed by summing the difference in elevations between all pixel pairs with a given pixel spacing to produce one observation of semi-variance. This is reported for all combinations of lag in x and y (τ_x, τ_y). Since the precision of semi-variance calculated using few observations is poor, this is carried out only for lags up to half the series width called the *distance of reliability* (Journel and Huijbregts, 1978). For a surface $Z(x,y)$ with dimensions $2N$ by $2M$, the two-dimensional semi-variogram $\gamma(\tau_x, \tau_y)$ is calculated according to:

$$\gamma(\tau_x,\tau_y) = \frac{1}{2(N-\tau_x)(M-\tau_y)} \sum_{i=1}^{N-\tau_x} \sum_{j=1}^{M-\tau_y} [Z(x_i+\tau_x, y_j+\tau_y) - Z(x_i,y_j)]^2. \quad (1)$$

It yields a value of γ for each combination of (τ_x, τ_y) up to $\tau_x = N - \tau_x$ and $\tau_y = M - \tau_y$ (i.e., the distance of reliability). Since:

$$\gamma(\tau_x,\tau_y) = \gamma(-\tau_x,-\tau_y) \quad \text{and} \quad (2)$$

$$\gamma(-\tau_x,\tau_y) = \gamma(\tau_x,-\tau_y), \quad (3)$$

if $\gamma(\tau_x, \tau_y)$ is evaluated for all $-N < \tau_x < N$ and $-M < \tau_y < M$, then it is possible to plot a semi-variogram surface with $\tau_x = 0$, $\tau_y = 0$ at the center. Here, the 2D semi-variogram reveals the dependence of scaling characteristics on direction, i.e., whether the surface is anisotropic.

Provided the elevation increments used to determine $\gamma(\tau_x, \tau_y)$ are normally distributed, the presence of linear segments along each direction indicate self-affine scaling from which a value for D can be calculated (see Burrough, 1983; Robert, 1988; Xu *et al.*, 1993). In this case, the slope of the semi-variogram is twice the Hausdorff-Besicovitch dimension (H) and;

$$D = 3 - H \quad (4)$$

such that $2 \leq D \leq 3$. As D increases, the surface becomes increasingly rough until it completely fills a three dimensional space at $D = 3$. Conversely, as D decreases, the

surface becomes increasingly smooth becoming a Euclidean surface at $D = 2$.

An important consideration when estimating D is the presence of first-order, non-stationarity or trend in the data. Trend is often present in elevation data since the roughness of a surface is usually superimposed on another surface whose scale is larger than the scale of the scene under investigation (Mandelbrot, 1967). Therefore, data are typically detrended by fitting a polynomial to the data and subtracting it from the surface. Opposing opinions exist on this issue since there is no clear distinction between removing trend and removing important roughness information. While some research has suggested that trend removal is customary to produce reliable estimates of D (Cressie and Hawkins, 1980), Armstrong (1986) has shown that it is not recommended as, in the case of soil transect data, removing trend does not impact upon the outcome of the semi-variogram. Thus, the effects of surface detrending on the outcome of scaling analysis were also investigated in this research.

Methodology

The work carried out for this research is discussed below in three sections: (a) artificial surface generation; (b) error simulation; and (c) scaling analysis and the estimation of D.

Artificial Surface Generation

In this experiment, errors were modeled numerically and applied to a surface under controlled conditions. In order to be able to control surface roughness for future experiments, the simulated errors were applied to an artificial surface whose roughness could be predetermined. This surface was designed to have similar fractal characteristics to a real surface whist having been generated independently of photogrammetric methods. In order to produce a realistic surface, a photogrammetrically generated DEM was used as the foundation for modeling. The data chosen for this purpose were collected in Glen Affric, Scotland and are discussed in more detail in Lane *et al.*, (2000). The spatial characteristics of the photogrammetrically-acquired DEM (i.e., scale, coordinate system, and relief) were adopted for the artificial surface. The block bundle adjustment parameters from the Glen Affric project, including the standard error of their estimates, were also used in the error simulation.

The artificial surface was generated following Russ (1994), which was based on fractal Brownian motion (fBM) using a variation of recursive midpoint displacement. The algorithm provides two user-defined parameters to control the characteristics of the resulting surface. The first (R) determines the spacing of the new set of points after each iteration where $0 \leq R \leq 1$. The second (α) controls the roughness of the surface in terms of D according to $D = 3 - \alpha$. For this experiment the default value of 0.5 was used for both R and α since:

1. Standard midpoint displacement (at $R = 0.5$) is known to be a simple, straightforward, and computationally efficient method for approximating fBM and overcomes the problem of non-stationarity (Peitgen and Saupe, 1988); and
2. At $\alpha = 0.5$, the influences of persistence (positive correlation, where elevation changes between points are more likely to have the same sign, $\alpha > 0.5$) and antipersistence (negative correlation, where elevation changes between points are more likely to have opposite signs, $\alpha < 0.5$) between data points could be minimized (Robert and Richards, 1988).

To investigate the role of trend in scaling analysis applications, two additional surfaces were required: one surface with first-order trend; and one surface with second-order trend. To do this, first- and second-order polynomials were fitted to the Glen Affric DEM to produce two realistic trend surfaces using the POLY2FIT algorithm of MATLAB, Version 6.5. Both first- and second-order trend were included in this experiment since the boundary between trend and surface features relevant to roughness is not well defined (Butler *et al.*, 2001). Thus, three artificial surfaces were used as the starting point of this experiment: the trend-free artificial surface; the surface with first-order trend; and the surface with second-order trend.

Error Simulation

In this stage of the experiment, errors were simulated numerically and applied to the three artificial surfaces described above. As noted previously, this investigation simulated elevation errors associated with: (a) uncertainty in camera position and orientation estimates; (b) uncertainty in the camera focal length; and (c) the performance of the stereo-matching algorithm in low texture areas. Although many sources of error are encountered in the photogrammetric process, these errors represent problems common to all digital photogrammetric applications. However, they are nonetheless quite different in nature. Whereas (a) is a general problem, (b) is common with semi-calibrated cameras or cameras with out-of-date calibration certificates, and (c) is frequently encountered when using automated DEM generation methods and poor imagery with a high signal-to-noise (SNR) ratio (i.e., low contrast).

In order to simulate the photogrammetric errors numerically, a program was developed to generate a set of image coordinates by working in reverse through the basic form of the collinearity equations, starting with a set of object-space coordinates that describe a surface. This required an input DEM, a set of exterior orientation parameters, and the corresponding camera focal length. These parameters could then be perturbed systematically under an approximated Gaussian distribution according to the standard error of their estimation (as determined in the Glen Affric project). In the case of simulating errors caused by automated data extraction routines in low SNR areas, the perturbation was applied directly to the image-space coordinates with sensor parameters left unchanged. Using perturbed values, new ground coordinates could be produced to give a new DEM containing the simulated error.

For each type of error, the parameters were perturbed randomly and repeated over several iterations (approximately 35) to achieve a sample of error surfaces that were representative in terms of magnitude and orientation under the specified standard errors. This produced about 105 surfaces in total. Since: (a) the scaling analysis routine is computationally intensive; and (b) the investigation did not call for detailed characterization of error, only two examples of each error type were selected to carry forward to the scaling analysis. The first was selected to represent relatively small errors (i.e., <1 standard deviation). The second was selected to represent relatively large errors (i.e., approximately 2 standard deviations). Overall, the above procedure resulted in 21 surfaces to which scaling analysis was applied. They included:

1. The original artificial surface;
2. The original artificial surface to which first-order trend was added;
3. The original artificial surface to which second-order trend was added; and
4. The two sample surfaces (i.e., one representing small errors and the other representing large errors) for each of the three types of errors that were modeled, and applied to each of (1), (2) and (3).

Table 1 lists these 21 surfaces and gives relevant details for each.

The effect of detrending on scaling analysis was assessed by applying first- or second-order detrending

TABLE 1. DETAILS OF THE ERROR SIMULATION SURFACES. ERROR VALUES GIVEN ARE (†)THE ROOT MEAN SQUARE VALUES FOR THE POSITIONAL/ORIENTATION ERRORS AND (‡)THE STANDARD DEVIATION OF ERROR

	Trend		
Error Type	None	First-Order	Second-Order
None	t_0	t_1	t_2
Small EO (0.212 m/0.0315°)†	t_0eo_S	t_1eo_S	t_2eo_S
Large EO (0.593 m/0.0724°)†	t_0eo_L	t_1eo_L	t_2eo_L
Small FL (3.706×10^{-5} m)	t_0fl_S	t_1fl_S	t_2fl_S
Large FL (7.933×10^{-5} m)	t_0fl_L	t_1fl_L	t_2fl_L
Small RE (0.071 m)‡	t_0re_S	t_1re_S	t_2re_S
Large RE (0.357 m)†	t_0re_L	t_1re_L	t_2re_L

(EO = exterior orientation; FL = focal length; RE = random elevation).

routines to all the surfaces to which both trend and error had been added. The scaling analysis was then applied. The detrending was carried out by fitting first- and second-order polynomials to the trended error surfaces, again using the POLY2FIT algorithm and subtracting them from each surface. The effects of both first- and second-order detrending were assessed because trend can exist over several orders of magnitude. Higher-order detrending was not applied because as the order of the detrending polynomial increases, the risk of removing important surface information also increases. Table 2 lists the 12 additional surfaces that were subject to scaling analysis for assessing the effects of detrending.

Scaling Analysis and the Estimation of *D*

The final step of the experiment was to produce 2D semi-variogram surfaces from which *D* could be estimated for all 33 DEMs produced in the preceding section. From these, estimates of the surfaces' fractal dimension could be derived. This was carried out using a program written explicitly for this experiment called 2DSVAR that calculates the semi-variance between elevations for lags in all directions according to Equation 1. The program produces a semi-variogram surface with lag in the *x* and *y* directions represented on the horizontal axes and semi-variance represented on the vertical axis.

The approach used to conduct the fractal analysis was developed in Carbonneau (2003). The routine extracts 1D profiles from a 2D semi-variogram, converts them to binary images and uses simple image processing techniques to detect linear segments. The output is a 2D semi-variogram and a fractal map with semi-variance and *D* plotted by direction, respectively. The image processing approach to

TABLE 2. DETRENDED SURFACES USED IN THE FRACTAL ANALYSIS

Error Surface ID	Detrended Surface ID	Order of Detrending
t_1eo_S	$t_1eo_Sd_1$	First
t_1eo_L	$t_1eo_Ld_1$	First
t_1fl_S	$t_1fl_Sd_1$	First
t_1fl_L	$t_1fl_Ld_1$	First
t_1re_S	$t_1re_Sd_1$	First
t_1re_L	$t_1re_Ld_1$	First
t_2eo_S	$t_2eo_Sd_2$	Second
t_2eo_L	$t_2eo_Ld_2$	Second
t_2fl_S	$t_2fl_Sd_2$	Second
t_2fl_L	$t_2fl_Ld_2$	Second
t_2re_S	$t_2re_Sd_2$	Second
t_2re_L	$t_2re_Ld_2$	Second

determining *D* from the 2D semi-variogram begins by applying simple convolution filtering to binary images generated from semi-variogram profiles in order to detect any linear segments in the profiles. To illustrate, the following kernel (K_{45}) can detect lines with an orientation of 45°:

$$K_{45} = \begin{pmatrix} -1 & -1 & 2 \\ -1 & 2 & -1 \\ 2 & -1 & -1 \end{pmatrix}. \quad (5)$$

Consider two 3×3 binary matrices (L_{45} and L_{90}) that represent two binary images (one with a 45° line and the other with a vertical line, respectively). These are given as:

$$L_{45} = \begin{pmatrix} 0 & 0 & 1 \\ 0 & 1 & 0 \\ 1 & 0 & 0 \end{pmatrix} \text{ and} \quad (6)$$

$$L_{90} = \begin{pmatrix} 0 & 1 & 0 \\ 0 & 1 & 0 \\ 0 & 1 & 0 \end{pmatrix}. \quad (7)$$

Convolving L_{45} and L_{90} with K_{45} gives:

$$K_{45} \otimes L_{45} = 6 \quad \text{and} \quad K_{45} \otimes L_{90} = 0. \quad (8)$$

This shows how convolving a line detection kernel (K_ω) with a binary image will yield a predictable maximum where a line of orientation ω is present. We refer to this value as the *detection threshold*.

When using small 3×3 kernels like L_{45} and L_{90}, only lines with orientations of 0°, 45°, and 90° can be detected. However, for the purpose of detecting linear sections in a semi-variogram profile, a higher angular resolution is required. Thus, the size of the convolution kernel was increased. This improves the angular resolution whilst simultaneously increasing the computational requirements of the convolution. Experimentation revealed that a kernel size of 50×50 produced an angular resolution of 1° with manageable computational demands. In the 50×50 line detection kernel, pixels on the line that corresponded to an angle of ω were set to 49 while the remainder of the matrix cells are set to -1 to conform to the kernel of zero-sum convention. When a 50×50 binary image containing a line of orientation ω is convolved with K_ω the result is 2450. The difference in convolution maxima for angles ω and $\omega + 1°$ is at least 1225 which allows for a reliable capacity for resolving angles ω and $\omega + 1°$.

The line detection kernels were applied to the 1D semi-variograms by converting them into binary images where those on the profile were represented by a 1 and those that were not were represented by a 0. The pixel dimensions of the binary profile image were dictated by the size of the kernel. Since a kernel window of 50×50 pixels was chosen, the linear sections in the semi-variogram image detected by this kernel will have a minimum length of 50 pixels. Thus, the minimum length detectable by the kernel will depend on the resolution of the image. Since the reliability of linear sections will decrease as the length of the section decreases, the author found that a minimal length of one-half order of magnitude could be reliably achieved. Thus, the image size of the semi-variogram was set to 200×200 pixels which produced the correct image resolution. Additionally, a buffer zone of zeros 50 pixels in width was added around the perimeter of the input images to insure that edge effects associated to the convolution process would not influence the results. However, round-off errors from the digitization produced minor imperfections in linear sections. These

imperfections meant that not all positive pixels in the detection kernel fell within the linear sections, which caused the line detection to fail. To combat this, morphological dilation was applied to the binary images. However, as dilation caused the alteration of the predicted detection threshold, it was necessary to recalculate this value.

Applying morphological dilation to L_{45} gives:

$$DL_{45} = \begin{pmatrix} 0 & 1 & 1 \\ 1 & 1 & 1 \\ 1 & 1 & 0 \end{pmatrix} \tag{9}$$

which, when convolved with K_{45}, gives:

$$K_{45} \otimes DL_{45} = 2. \tag{10}$$

In the dilated image, each off-diagonal value has reduced the convolution result by 1. Thus, to predict the detection threshold in a dilated image, the off-diagonal pixels must be counted. This can be accomplished using an identity convolution filter. Convolving DL_{45} with a 3×3 identity matrix gives:

$$DL_{45} \otimes I_3 = 7. \tag{11}$$

Since there are nine pixels in total and three along the diagonal in DL_{45}, Equation 11 reveals that four pixels are off the diagonal. Thus, the detection condition for linear sections can be generalized as:

$$K \otimes DL \geq (SK)^2 - I_{SK} \otimes DL \tag{12}$$

where K is the line detection kernel, DL is the dilated binary line image, SK is the size of the detection kernel in pixels, and ISK is an identity matrix of size SK. Equation 12 yields an exact threshold value for each $SK \times SK$ area. Each point that satisfied the condition represented a detected linear section of length SK. Thus, linear sections of length I pixels, where $I > SK$, will have $I - SK$ pixels that satisfy the condition. To identify linear sections or varying orientations, the convolution is repeated with detection kernels for angles ranging from 0° to 90°, in increments of 1°. However, since the morphological dilation of the binary semi-variogram profile images added an element of uncertainty to the profile and thus a slight tolerance to curvature, statistical testing was required. Linear regression was used to test the linearity of identified bands and an f-test was applied to test the significance of any discrepancies.

One of the benefits of the routine was that no *a priori* knowledge was required about the number of linear segments present, their location within the profile, or their slope. This allowed fractal characteristics such as multifractals and anisotropy to be identified reliably, without confusion with those zones with unreliable fractal structure due to insufficient observations of semi-variance (zones of unreliability). An example of the program's output is given in Figure 1 which shows the results for the artificial surface used here (t_0). The undulation of the edges of both the semi-variogram and fractal maps is a product of the DEM's rectangular shape and the gridded sampling pattern. While the analysis itself was carried out using color semi-variogram and fractal maps, grayscale figures have been used for the purposes of publication. Additionally, as the directional semi-variogram plots are not discussed further in this paper, they have been omitted from the remaining figures in the text.

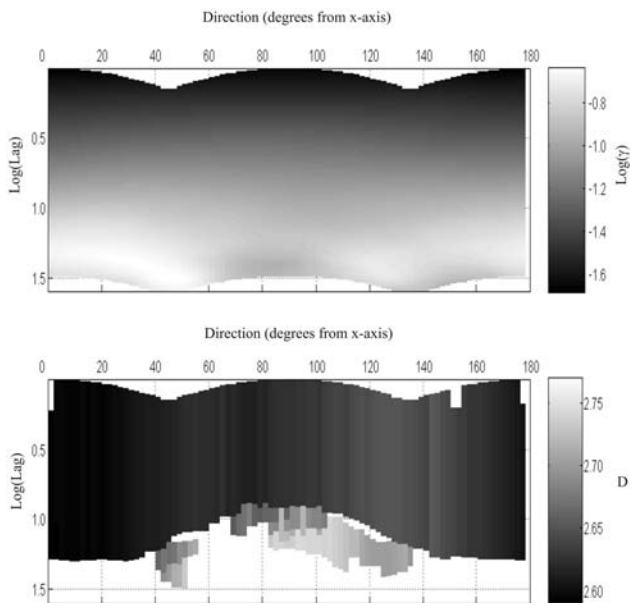

Figure 1. An example of the directional semi-variogram and fractal map produced using the original artificial surface used in this experiment. Note that the directional semi-variogram is included here to show the relationship between the directional semi-variogram and the fractal map. It will not be included in subsequent figures.

Results

Figure 2 shows the DEM that was generated for this experiment (Figure 2a) and the photogrammetrically-generated DEM upon which it was modeled (Figure 2b). As the software generates surfaces with zero mean (i.e., no first-order trend), the measured DEM was detrended so the DEMs could be compared. Figure 2 shows how these surfaces would have different values of D with the artificial surfaces being somewhat rougher (i.e., with a higher value of D). However, this was unavoidable due to the decision to generate the surface using $\alpha = 0.5$ to minimize the influences of strong persistence and antipersistence. The two trend surfaces that were generated from the Glen Affric data to assess the role of trend are given in Figure 3. These surfaces were added to the artificial DEM in Figure 2a to give the two DEMs in Figure 4. The three resulting DEMs were the starting point of the experiment presented in this paper.

The output of the numerical error modeling can be observed by plotting the error surfaces that were generated in 3D. The error surfaces shown in Figure 5 and described in Table 3 represent the sample of error surfaces that were carried forward to the scaling analysis stage of the experiment. The plots on the left side (Figure 5a, 5c, and 5e) represent typically small errors (i.e., <1 standard deviation) while those on the right side (Figure 5b, 5d, and 5f) represent larger errors (i.e., approximately 2 standard deviations). The simulation produced two types of errors: systematic errors corresponding to error in exterior orientation and focal length that could be described with a first-order polynomial (Figure 5a through 5d); and random error corresponding to random image coordinate errors that could be described stochastically (Figure 5e and 5f). An important observation at this stage is the non-linear relationship between the magnitude of the exterior orientation parameter perturbation and the resultant surface error. Whereas the small exterior orientation errors resulted in surface elevation errors that averaged 0.523 m, the large errors, roughly double that of the smaller error, resulted in surface elevations errors that averaged −6.019 m. This type of relationship was not seen

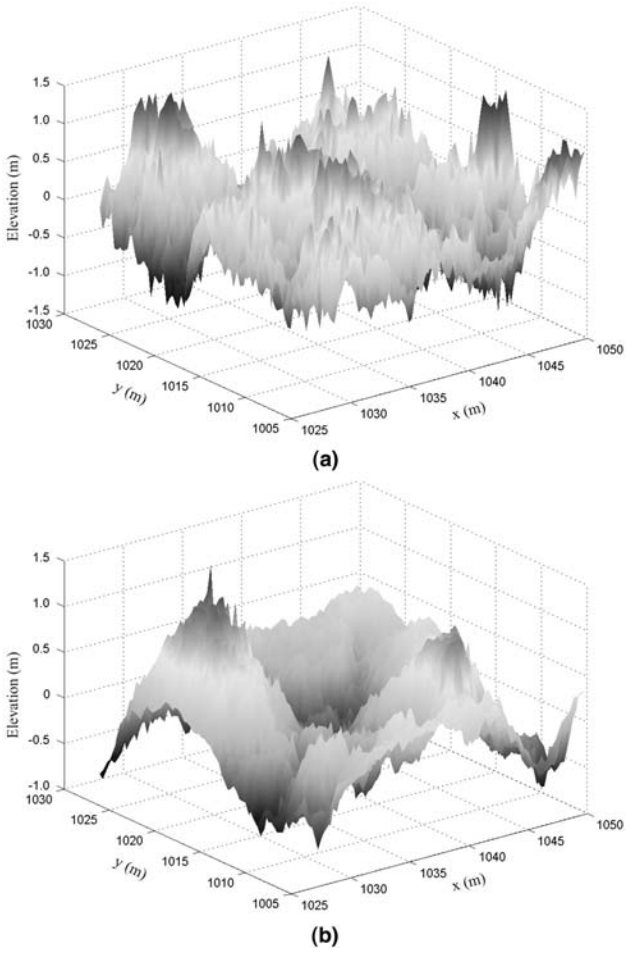

Figure 2. (a) The artificial fractal surface that formed the basis of this experiment; and (b) the detrended Glen Affric field site surface model.

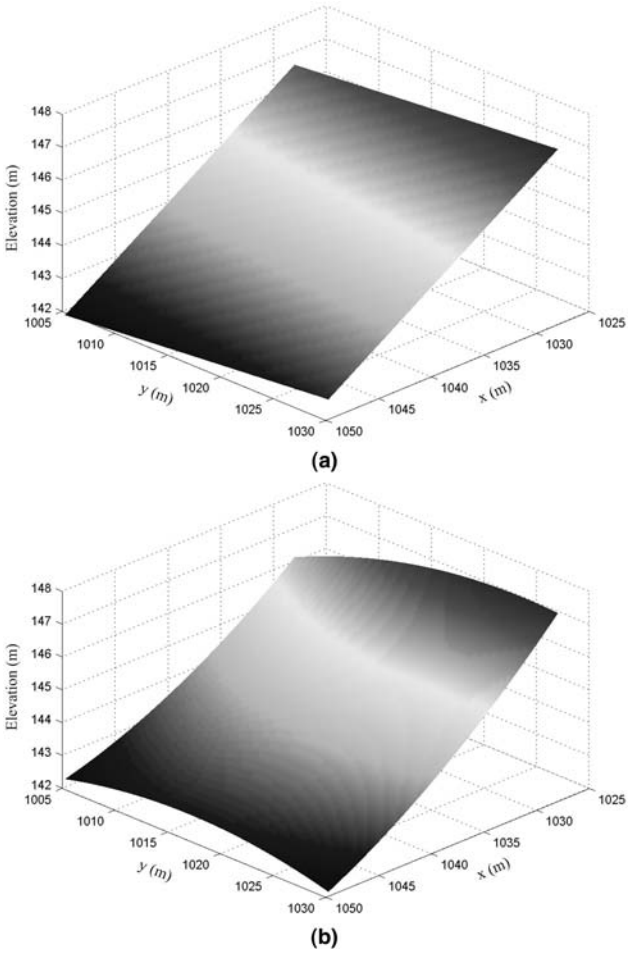

Figure 3. (a) First-order; and (b) second-order trend surfaces derived from the Glen Affric DEM.

with the focal length or random elevation errors, and shows that small additional degradation of exterior orientation error may propagate through to much larger scale surface errors.

The directional semi-variogram and the fractal map of the original trend- and error-free surface (t_0) (Figure 1) show that the artificial surface is largely isotropic, more clearly in Figure 1b than in Figure 1a, with D varying only slightly with direction between about 2.58 and 2.65. The discrepancy between the value of D here and the value of 2.50 as predicted by the assignment $\alpha = 0.5$ is not surprising since the estimation of D is highly dependent on both the method used to make the estimation as well as the method used to generate the fractal surfaces (Russ, 1994). However, for comparing relative changes between the fractal characteristics of a surface, the absolute determination of D is not necessary. The fractal map also clearly shows what will be referred to as the *zone of unreliability*. This is an area along the bottom of the map (large lags) where the estimates of D may be unreliable due largely to the comparatively small number of observations used in the calculations. In this case, this zone is distinct from the surface's main fractal structure which enables confidence to be placed in the results from the stable part of the fractal map.

As expected, the introduction of systematic errors to the original surface had minimal effect on the scaling characteristics of the surface. This suggests that scaling characteristics will be insensitive to photogrammetric errors where the errors generated produce trend-like elevation errors. In strong contrast, the random elevation errors proved to have a considerable effect on the fractal characteristics of the surface even when the error was relatively small. Figure 6 gives the semi-variograms and fractal maps of the original surface after the addition of the random errors. Where the error was relatively small (Figure 6a), the surface saw an overall increase in roughness and the surface became more anisotropic. Also, multifractal bands appeared in the fractal map where only singular bands had previously been identified. Overall, the fractal structure began to disintegrate at both high and low lags and the zone of unreliability became larger and less well defined. Where the error was somewhat larger (Figure 6b), the fractal structure of the surface completely disintegrated leaving no trace of the fractal structure of the original surface.

Figure 7 gives the fractal maps of the original surface after the addition of the first- and second-order trend shown in Figure 3. Contrary to the results suggested above, these results illustrate that the interpretation of a surface's scaling characteristics are highly sensitive to trend but only when the slope is of comparable scale to the relief of the surface. This is potentially important for surfaces of low relief (e.g., floodplains) where even the systematic errors like those in

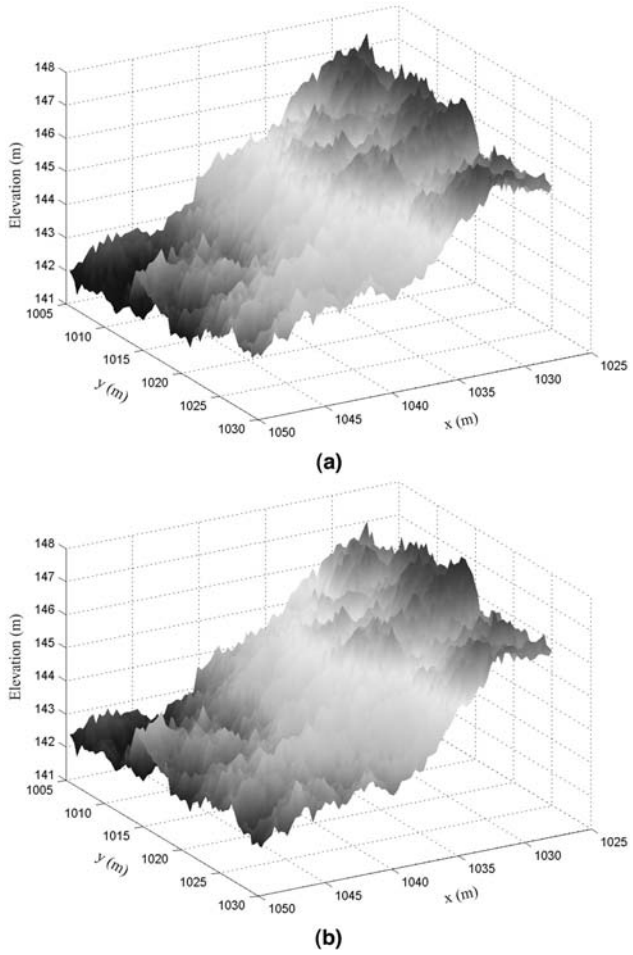

Figure 4. The artificial surface after incorporating: (a) the first-order; and (b) the second-order trend surfaces from Figure 3.

Figure 5a through 5d could significantly affect the outcome of a scaling analysis. Comparison of these maps with that of the original surface reveals that surface trend causes: (a) a substantial decrease in roughness of the surface with the greatest effect occurring in the direction of maximum slope; (b) the degradation of the fractal structure at high and low lags; (c) an increase in the extent of the zone of unreliability accompanied by a decrease in its distinctness from the main fractal structure; (d) an increase in surface anisotropy; and (e) the appearance of mixed fractal bands. This was true for both first- and second-order trend. However, with the latter, portions of the fractal map disappeared completely. This suggested that the power law structure of the semi-variogram surfaces was lost over the entire range of lags. A similar result was found when the random errors were added to the surfaces with trend.

The effects of detrending on the scaling characteristics of the different surfaces are revealed in Figure 8 and Figure 9, which give the results of the surfaces containing systematic error, and Figure 10 and Figure 11, which give the results of the surfaces with random error. Comparison of these results with the fractal map of the original surface in Figure 1 showed how first- and second-order detrending tended to remove the effects caused by these errors though the degree of removal depended largely on the nature of the error itself. In the case of systematic errors, first-order detrending made some progress towards restoring the original fractal structure from the effects of both trend and error, though remnants still existed at high and low lags (Figure 8). This suggests that the presence of error, though having minimal effect on the scaling characteristics of the surface, will play some role in prohibiting the removal of the first-order trend, or the scaling characteristics would have been restored to its pre-trend state. However, this role will depend on the relative orientation of the error surface to the surface itself. When second-order detrending was applied, the resulting fractal maps were identical to those for the original surface (Figure 9). In other words, the second-order detrending removed all traces of the effects of both the second-order trend and the error. This highlights the benefits of detrending a DEM with a second-order polynomial prior to conducting any kind of scaling analysis.

In the case of the random elevation errors, as expected the effect of detrending on the surface's fractal structure was minimal since the errors that were introduced cannot be described using a polynomial. Comparing Figure 10 and Figure 1 revealed that, in the presence of small random errors, the first-order detrending routine made some progress towards restoring the fractal structure of the surface. However, as detrending will highlight high-frequency information in a data set, the random errors caused the emergence of several mixed fractal bands and one area where the fractal structure disappeared completely. Additionally, the surface maintained a higher value of D than the original surface. Notice also how the zone of unreliability merged with the main fractal structure of the surface making it more different to identify. With the large random errors, the first-order detrending had no effect.

Finally, Figure 11 shows the fractal maps of the same two surfaces after second-order detrending. This time the second-order polynomial was even more successful at restoring the fractal structure of the surface in the presence of the small random errors and the zone of unreliability even became distinct. However, mixed fractal bands were still present and the surface still showed a higher value of D as compared to the original surface. With the large random errors, the second-order detrending again had no effect.

Discussion

The numerical modeling of the selected photogrammetric errors produced both systematic errors caused by the random perturbation of the exterior orientation parameters and the focal length, and random errors caused by the perturbation of the image coordinates. Although the systematic errors had little effect on the scaling characteristics of the surface, the non-linear nature of the relationship between the magnitude of the parameter uncertainty and the resultant magnitude of the error surface is noteworthy for photogrammetry in general. In photogrammetric data collection, the elements of interior and exterior orientation are adjusted during the bundle adjustment and constrained by the uncertainty of their estimation which is typically a user-defined parameter. Understandably, the over- or under-estimation of these values can have an important influence on the results of the adjustment. Overestimating the uncertainty under-constrains the model producing a better fit statistically but at the possible expense of accuracy. Underestimating the uncertainty has the opposite effect. However, the non-linear relationship demonstrated between the magnitude of parameter uncertainty and the magnitude of the consequent error surface suggests that the consequences on data

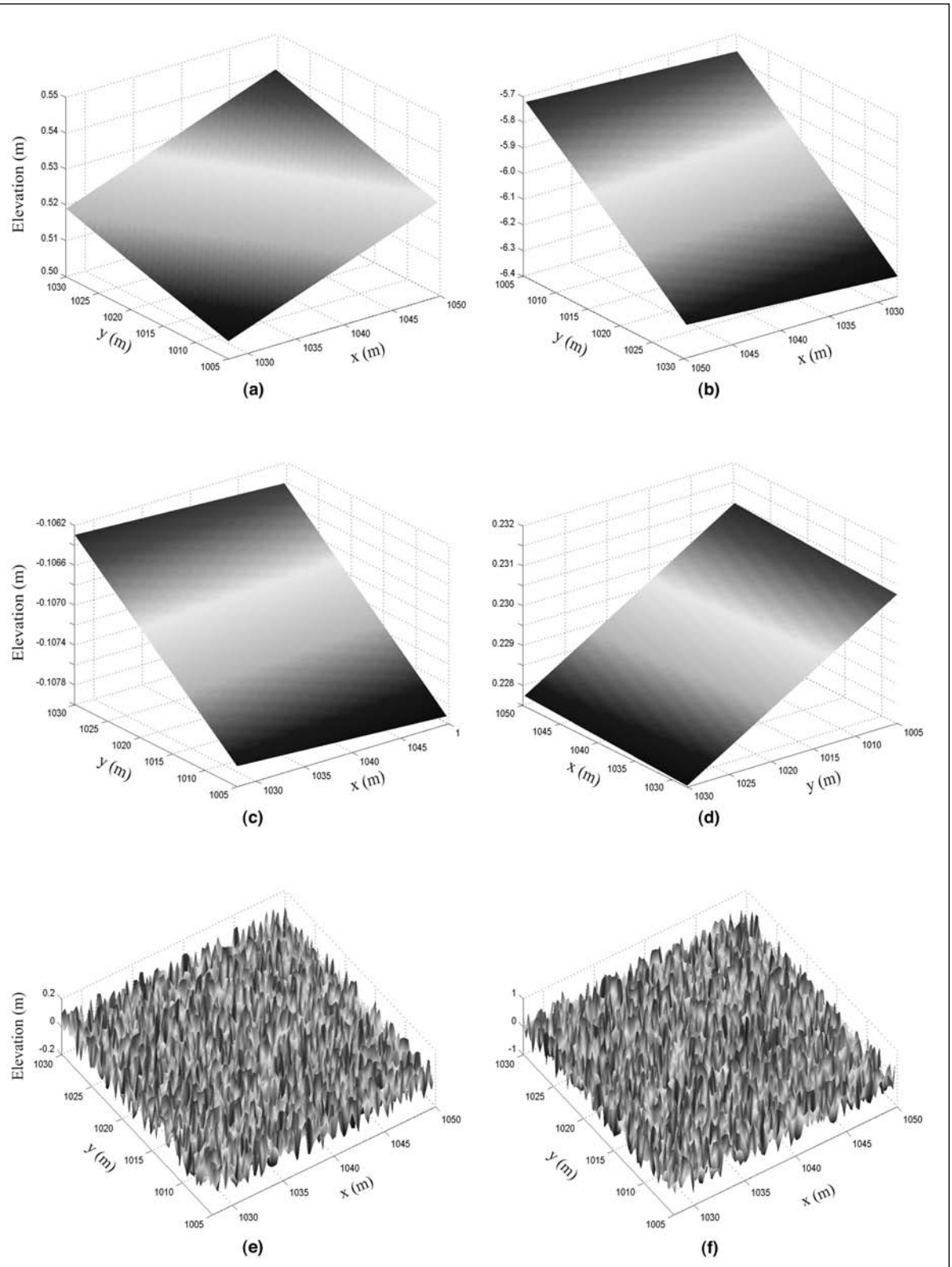

Figure 5. Plots of the error surfaces caused by the exterior orientation errors in (a) and (b); the focal length errors in (c) and (d); and the random elevation errors in (e) and (f). The plots in the left hand column represent a sample of typically small errors (i.e., <1 standard deviation) while those in the right hand column represent larger errors (i.e., approximately 2 standard deviations).

TABLE 3. SUMMARY STATISTICS OF THE ERROR SURFACES WITH SMALL ERRORS REPRESENTING DEVIATIONS BELOW 1 STANDARD DEVIATION AND LARGE ERRORS REPRESENTING DEVIATIONS AROUND 2 STANDARD DEVIATIONS

Error Surface	Minimum (m)	Maximum (m)	Mean (m)	Standard Deviation (m)
EO_S (Figure 5a)	0.505	0.540	0.523	n/a
EO_L (Figure 5b)	−6.322	−5.725	−6.019	n/a
FL_S (Figure 5c)	−0.108	−0.106	−0.107	n/a
FL_L (Figure 5d)	0.228	0.231	0.229	n/a
RE_S (Figure 5e)	−0.122	0.122	0.003	0.071
RE_L (Figure 5f)	−0.610	0.609	0.002	0.357

(EO = exterior orientation; FL = focal length; RE = random elevation).

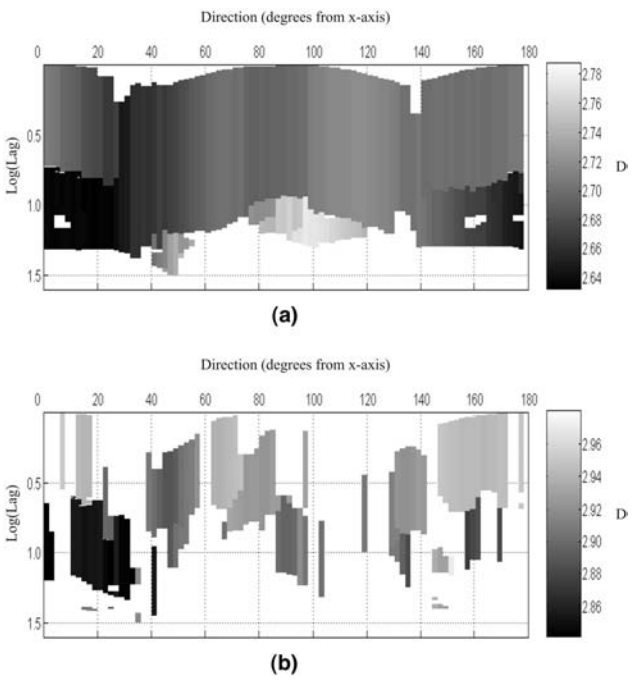

Figure 6. Fractal maps of the original surface after the introduction of random elevation errors of: (a) small; and (b) large magnitude.

quality of under-constraining a model may be greater than over-constraining a model.

In strong contrast to the systematic errors, the surface's fractal structure was understandably highly sensitive to random errors. Even where errors were relatively small, the fractal structure of the surface quickly disintegrated, thus minimizing the reliable information obtainable from the scaling analysis. Of even greater concern is the fact that these random errors caused changes in the fractal structure of the surface that mimicked characteristics that have been found to occur in nature. For example, the anisotropy and mixed fractal bands seen in Figure 6 could easily be interpreted as artifacts of natural processes rather than the result of errors. Therefore, it is of paramount importance that *a priori* evidence for the existence of such features exist before reaching such conclusions (i.e., Butler *et al.*, 2001). These results also raise questions about the interpretability of scaling analysis in the absence of robust quality assessment and highlight the importance of assessing either the theoretical

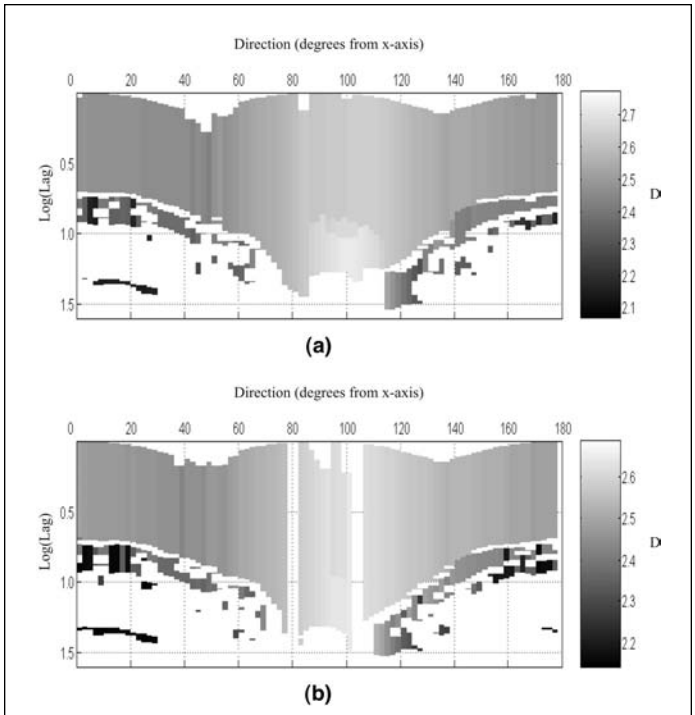

Figure 7. Fractal maps of original surface with: (a) first-order trend; and (b) second-order trend.

or the measured non-systematic error in a surface. This paper has presented a useful means for achieving this through numerical error simulation.

As well as revealing information about how random errors affect the results of scaling analysis, these results also have important methodological implications for how a scaling analysis should be conducted and interpreted. First, the results have shown that the presence of surface trend has a considerable effect on the outcome of scaling analysis (Figure 7). This lends support to the argument that the detrending is required in order to derive reliable estimates of *D* (Cressie and Hawkins, 1980) and opposes Armstrong (1986)'s position that it may not be necessary. Unfortunately, the effects go beyond simply causing a change in the overall representation of the roughness of the surface. As was found with random elevation errors, trend produced the same artifacts that are thought to be produced by natural processes such as anisotropy and mixed fractal bands. This brings the credibility of scaling analysis as a whole into question where the role of trend has not been thoroughly addressed, since the cause of the scaling properties observed in the semi-variogram may be uncertain. The strong influence of trend on scaling analysis shows that, although the distinction between trend and important surface features is not well defined, it is important that the goals and limitations of scaling analysis are well defined.

In terms of detrending, the results have shown that the success of detrending at removing the scaling effects of trend depends largely on the nature of error in the DEM. While first-order detrending failed to remove the effects of trend in the presence of systematic error common in photogrammetric data, second-order detrending did effectively remove the effects of both, irrespective of the magnitude of the error. However, in the presence of random errors, the ability of detrending to remove the effects of trend was limited. Even with only small random errors the detrending could not completely remove the effects of trend on the

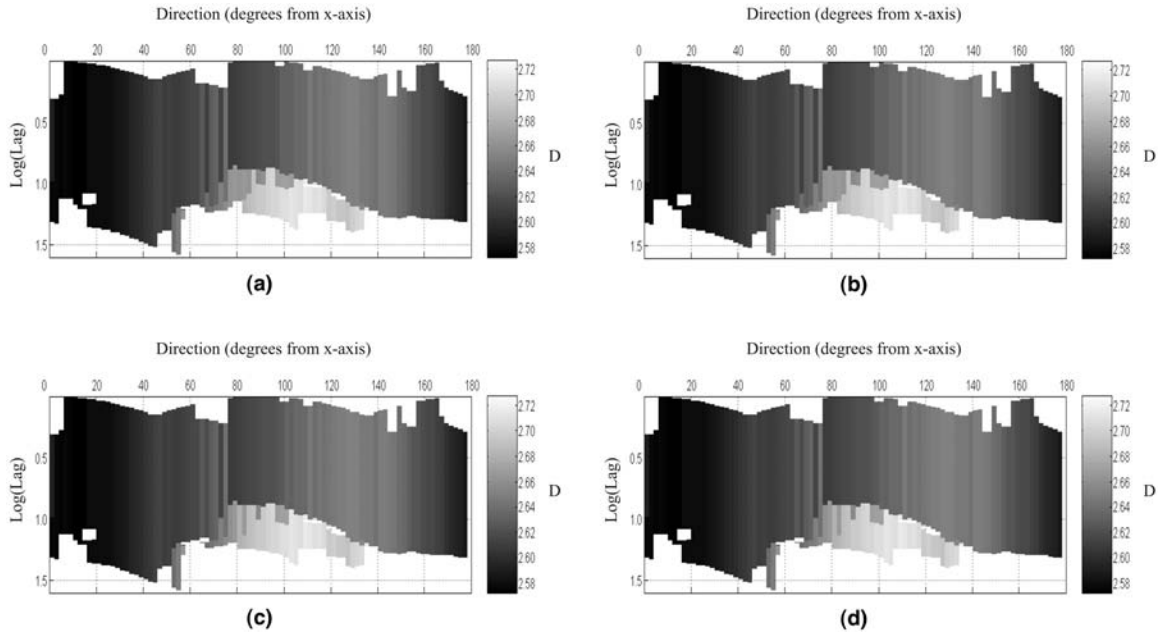

Figure 8. Fractal map of first-order trended surface containing: (a) small; and (b) large exterior orientation errors; and (c) small; (d) and large focal length errors after first-order detrending.

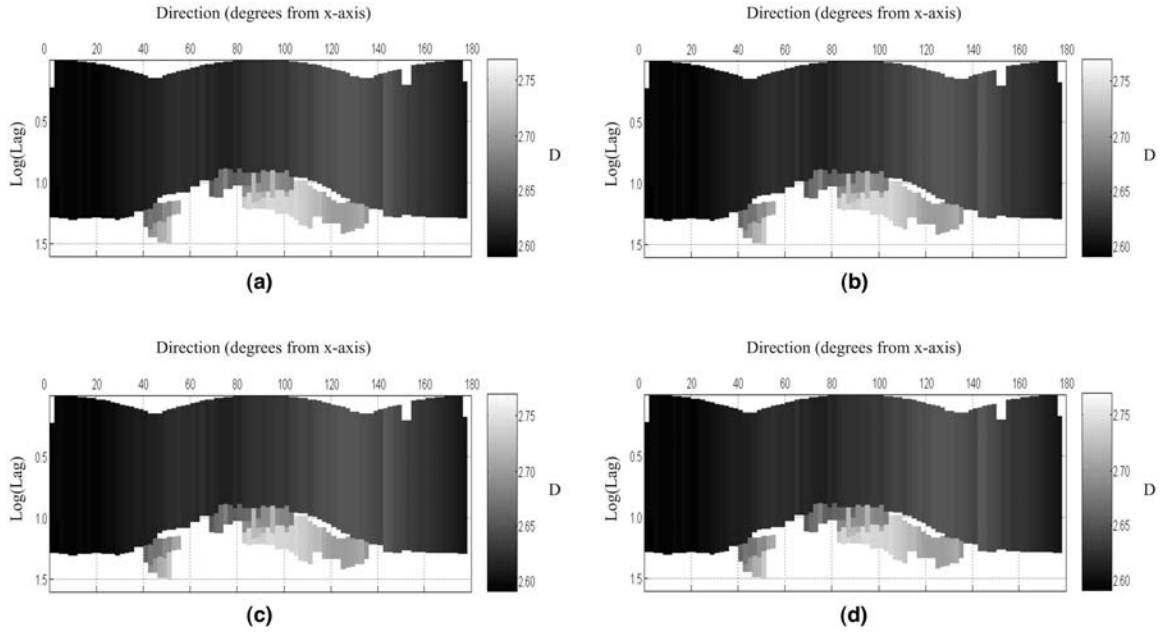

Figure 9. Fractal map of second-order trended surface containing: (a) small; and (b) large exterior orientation errors; and (c) small; (d) and large focal length errors after second-order detrending.

surface's scaling properties though some improvement was seen. With large errors, the detrending had no effect. While the importance of applying second-order detrending prior to scaling analysis is clear, an important weakness of scaling analysis has been highlighted. Even when non-systematic errors are sufficiently small to have minimal effect on the scaling structure of the surface, the results may be still be unreliable since their presence can inhibit the complete removal of surface trend.

A final point worth discussing is the performance of the 2D semi-variogram and fractal map method that was used in this research for estimating *D*. This research has shown that the approach proved to be a useful method for carrying out scaling analysis. While simple to implement, the resultant estimates of

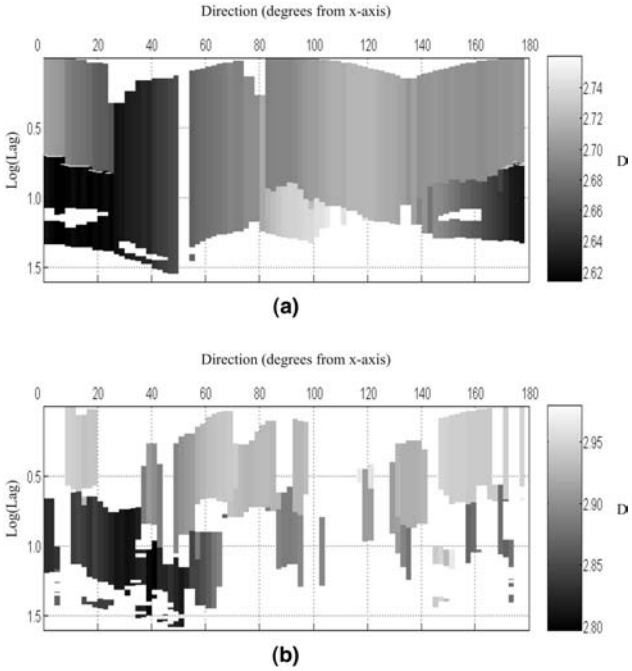

Figure 10. Fractal map of first-order trended surface containing: (a) small; and (b) large random errors after first-order detrending.

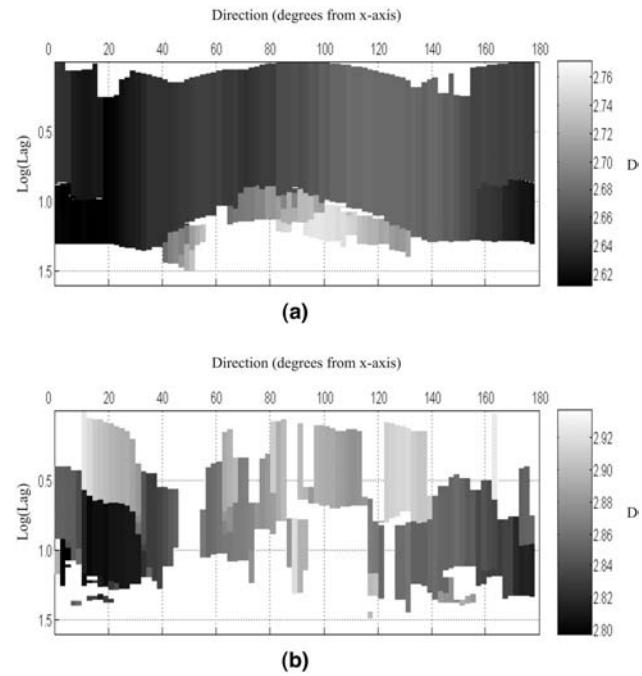

Figure 11. Fractal map of second-order trended surface containing: (a) small; and (b) large random errors after second-order detrending.

D were reliable having passed though statistical significance testing and the graphical 2D output enabled easy identification of important scaling features such as anisotropy and multifractals and also of the scales across which the estimates of *D* were reliable. These characteristics are especially important for scaling analysis carried out on natural surfaces.

Conclusion

This paper has presented the results of an investigation into the effects that can be expected when common DEM error, including those associated with perturbation of the camera exterior orientation, focal length and DEM image coordinates, propagate through a scaling analysis. Included in this investigation was the role of detrending, which was deemed important since the role of trend and detrending in scaling analysis is not yet established in the literature. The paper demonstrated both the importance of error analysis, especially when employing novel methods of data processing and the value of the two dimensional scaling algorithm. The results showed that uncertainty in exterior orientation parameters and focal length caused systematic errors, which had little influence on the scaling characteristics of the surface. The effect of these errors was easily removed using second-order detrending. However, random errors had a strong influence on the scaling characteristics of the surface, and their presence interfered with the successful removal of the effects of trend even when they were relatively small. Of particular concern was the similarity of the artifacts caused by random elevation errors and trend to those believed to be associated with real fractal characteristics (i.e., mixed fractals and anisotropy). This finding cast doubt on the authenticity of the results of scaling analysis that show mixed fractal and anisotropy when based upon automatically-generated digital elevation models in the absence of other evidence (theoretical or empirical) to suggest their existence. Thus, before scaling analysis applications can be used to make any conclusions about a surface, a robust quality assessment is required to determine whether the results reflect the characteristics of error or of the surface itself. While this paper has demonstrated the importance of an investigation such as this, there is a clear need to expand this type of research into other types of DEM errors, surface characteristics, data sources, and methods of analysis.

Acknowledgments

The authors would like to thank those who made this research possible. Timothy D. James was funded by a School of Geography studentship held at the University of Leeds, UK, and Patrice E. Carbonneau was funded by an NATEQ studentship held at the INRS Eau, Terre et Environment in Quebec, Canada. Thanks also to Stuart Barr, Tavi Murray, Jim Chandler, and the two anonymous reviewers for their input.

References

Armstrong, A.C., 1986. On the fractal dimensions of some transient soil properties, *Journal of Soil Science*, 37(4):641–652.

Biham, O., O. Malcai, D. Lidar, and D. Avnir, 1998. Is nature fractal – Reply, *Science*, 279(5352):785–786.

Burrough, P.A., 1981. Fractal dimensions of landscapes and other environmental data, *Nature*, 294(5838):240–242.

Burrough, P.A., 1983. Multiscale sources of spatial variation in soil – The application of fractal concepts to nested levels of soil variation, *Journal of Soil Science*, 34(3):577–597.

Butler, J.B., 1999. *High Resolution Photogrammetric Monitoring and Analysis of the Structure of Gravel-bed River Surfaces*, University of Cambridge, Cambridge, 311 p.

Butler, J.B., S.N. Lane, and J.H. Chandler, 2001. Characterisation of the structure of river-bed gravels using two-dimensional fractal analysis, *Mathematical Geology*, 33(3):301–330.

Carbonneau, P.E., 2003. *Caractérisation Quantitative des Graviers Fluviaux pour la Modélisation de la Disponibilité d'Interstices Utilisables par le Saumon Atlantique (Salmo salar) Juvénile en Comportement Hivernal*, Ph.D. dissertation, INRS-ETE, Quebec City, Quebec, Canada, 203 p.

Carbonneau, P.E., S.N. Lane, and N.E. Bergeron, 2003. Cost-effective non-metric close-range digital photogrammetry and its application to a study of coarse gravel river beds, *International Journal of Remote Sensing*, 24(14):2837–2854.

Cressie, N., and D.M. Hawkins, 1980. Robust estimation of the variogram, *Mathematical Geology*, 12(2):115–125.

David, M., 1977. *Geostatistical Ore Reserve Estimation*, Elsevier, Amsterdam, 364 p.

Gong, J., Z. Li, Q. Zhu, H. Sui, and Y. Zhou, 2000. Effects of various factors on the accuracy of DEMs: An intensive experimental investigation, *Photogrammetric Engineering & Remote Sensing*, 66(9):1113–1117.

Goodchild, M.F., and D.M. Mark, 1987. The fractal nature of geographic phenomena, *Annals of the Association of American Geographers*, 77(2):265–278.

Griffiths, G.A., 1989. Form resistance in gravel channels with mobile beds, *Journal of Hydraulic Engineering*, 115(3):340–355.

Helmlinger, K.R., P. Kumar, and E. Foufoula-Ggeorgiou, 1993. On the use of digital elevation model data for Hortonian and fractal analyses of channel networks, *Water Resources Research*, 29(8): 2599–2613.

Heuvelink, G.B.M., 1998. *Error Propagation in Environmental Modeling with GIS*, Taylor and Francis, London, 127 p.

Hey, R.D., 1988. Bar form resistance in gravel-bed rivers, *Journal of Hydraulic Engineering*, 105(HY4):365–379.

Hobson, R.D., 1972. Surface roughness in topography: A quantitative approach, *Spatial Analysis in Geomorphology* (R.J. Chorley, editor), Methuen and Company, London, pp. 221–245.

Huang, Y.D., 2000. Evaluation of information loss in digital elevation models with digital photogrammetric systems, *The Photogrammetric Record*, 16(95):781–791.

Hunter, G.J., and M.F. Goodchild, 1997. Modeling the uncertainty of slope and aspect estimates derived from spatial databases, *Geographical Analysis*, 29(1):35–49.

Journel, A.G., and C. Huijbregts, 1978. *Mining Geostatistics*, Academic Press, London, 600 p.

Klinkenberg, B., 1994. A review of methods used to determine the fractal dimension of linear features, *Mathematical Geology*, 26(1):23–46.

Klinkenberg, B., and M.F. Goodchild, 1992. The fractal properties of topography: A comparison of methods, *Earth Surface Processes and Landforms*, 17(3):217–234.

Lane, S.N., T.D. James, and M.D. Crowell, 2000. Application of digital photogrammetry to complex topography for geomorphological research, *The Photogrammetric Record*, 16(95): 793–821.

Lee, J., P.K. Snyder, and P.F. Fisher, 1992. Modeling the effect of data errors on feature-extraction from digital elevation models, *Photogrammetric Engineering & Remote Sensing*, 58(10): 1461–1467.

Mandelbrot, B.B., 1967. How long is the coast of Britain? Statistical self-similarity and fractional dimension, *Science*, 156:636–638.

Mandelbrot, B.B., 1982. *The Fractal Geometry of Nature*, Freeman, San Francisco, California, 480 p.

Mark, D.M., and P.B. Aronson, 1984. Scale-dependent fractal dimensions of topographic surfaces – An empirical-investigation, with applications in geomorphology and computer mapping, *Journal of the International Association for Mathematical Geology*, 16(7):671–683.

Nikora, V.L., D.G. Goring, and B.J.F. Briggs, 1998. On gravel-bed roughness characterization, *Water Resource Research*, 34(3): 517–527.

Oliver, M.A., and R. Webster, 1986. Semi-variogram for modelling the spatial pattern of landform and soil properties, *Earth Surface Processes and Landforms*, 11(5):491–504.

Peitgen, H.O., and D. Saupe, 1988. *The Science of Fractal Images*, Springe, London, 312 p.

Robert, A., 1988. Statistical properties of sediment bed profiles in alluvial channels, *Mathematical Geology*, 20(3):205–225.

Robert, A., 1991. Fractal properties of simulated bed profiles in coarse-grained channels, *Mathematical Geology*, 23(3):367–382.

Robert, A., and K.S. Richards, 1988. On the modelling of sand bedforms using the semivariogram, *Earth Surface Processes and Landforms*, 13(5):459–473.

Roy, A., G. Gravel, and C. Gauthier, 1987. Measuring the dimension of surfaces: A review and appraisal of different methods, *Proceedings of the 8th International Symposium on Computer-Assisted Cartography (Auto-Carto 8)*, Baltimore, Maryland, pp. 68–77.

Russ, J.C., 1994. *Fractal Surfaces*, Plenum Press, New York, 309 p.

Suzuki, M., 1984. Finite-size scaling for transient similarity and fractals, *Progress in Theoretical Physics*, 71:1397–1400.

Tate, N.J., 1998. Estimating the fractal dimension of synthetic topographic surfaces, *Computers & Geosciences*, 24(4):325–334.

Weissel, J.K., L.F. Pratson, and A. Malinverno, 1994. The length-scaling properties of topography, *Journal of Geophysical Research-Solid Earth*, 99(B7):13997–14012.

Wen, R., and R. Sinding-Larsen, 1997. Uncertainty in fractal dimension estimated from power spectra and variograms, *Mathematical Geology*, 29(6):727–753.

Wise, S.M., 1998. The effects of GIS interpolation errors on the use of digital elevation models in geomorphology, *Landform Monitoring, Modelling and Analysis* (S.N. Lane, K.S. Richards, and J.H. Chandler, editors), Wiley, Chichester, pp. 139–164.

Wolf, P.R., and B.A. Dewitt, 2000. *Elements of Photogrammetry with Applications in GIS*, McGraw-Hill, New York, 608 p.

Xu, T., I.D. Moore, and J.C. Gallant, 1993. Fractals, fractal dimensions and landscapes – A review, *Geomorphology*, 8(4):245–262.

(Received 15 February 2005; accepted 04 August 2005; revised 10 October 2005)